Available online at www.sciencedirect.com

ScienceDirect

journal homepage: http://www.elsevier.com/locate/acme

Review

# Friction stir processing – State of the art

*Marek Stanisław Węglowski*

*Instytut Spawalnictwa (Institute of Welding), Bl. Czeslawa Str. 16-18, Gliwice 44-100, Poland*

ARTICLE INFO

*Article history:*
Received 7 September 2016
Accepted 1 June 2017
Available online 14 July 2017

*Keywords:*
Friction stir processing
Forces
Microstructure refinement
Friction stir alloying
Ultrasonic assisted friction stir processing

ABSTRACT

Increasing demands for operating properties of fabricated elements on one hand, and a necessity of reducing mass of a structure on the other, triggers materials engineering research into producing surface layers representing required functional properties. Methods commonly used in the production of surface layers, such as surfacing, spraying or re-melting with a laser beam have been known for years. A new method is the friction stir processing (FSP) of surface layers. The FSP process is primarily used for the modification of microstructure in near-surface layers of processed metallic components. In particular, the process may produce: fine grained structure, surface composite, microstructural modification of cast alloys, alloying with specific elements, improvement of welded joints quality. The chapter is composed of a few main parts. In the first part, based on literature review the main application and achievements of FSP processes are presented. In the second part: analysis of the process. The third part is focused on microstructure refinement and the last part provide information about friction stir alloying as well as friction stir processing with ultrasonic vibration.



## 1. Introduction

Friction stir processing (FSP) utilizes the same process principles as FSW (friction stir welding) [1]; however, instead of joining samples together the process modifies the local microstructure of monolithic specimens to achieve specific and desired properties by surface modifying the microstructure (Fig. 1). As in FSW, the tool induces plastic flow during the process, but depending on the selection of process parameters, i.e. applied force, travelling speed and rotational speed, the material flow can yield a modified microstructure that is beneficial to the performance/requirement of the material. Developed by Mishra in 2000, the modified process is a relatively new and exciting technique for microstructural development and modification as well as property enhancement [2].

During the FSP process, a pin is plunged into the modified material with the shoulder of the rotating tool abutting the base metals. As the tool (Fig. 1) transverses the modified direction, the rotation of the shoulder under the influence of an applied load heats the metal surrounding the modified area and with the rotating action of the pin induces metal from each section to flow and form the modified area. The microstructure that evolves during FSP results from the influence of material flow, plastic deformation and elevated temperature and is characterized by a central stir zone surrounded by a thermomechanically affected zone (TMAZ) and heat affected zone (HAZ). The deformed material is transferred from the retreating side (RS) of the tool pin to the advancing side (AS) and is forged by the tool shoulder, resulting in a solid state modification of the material. In the FSP process the most important area is between stir zone and

E-mail address: marek.weglowski@is.gliwice.pl.
http://dx.doi.org/10.1016/j.acme.2017.06.002

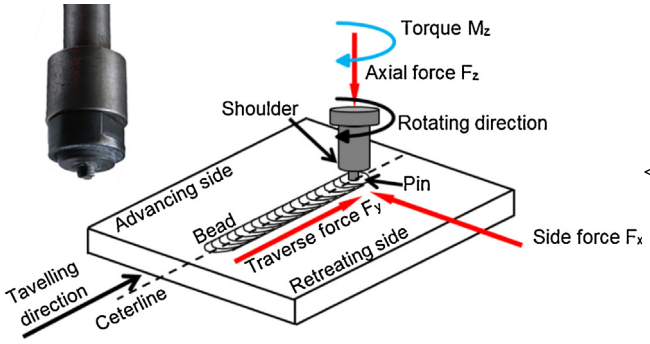


**Fig. 1 – Schematic drawing of friction stir processing process and a tool.**

thermomechanically affected zone. This area will determine properties of modified area, especially adhesion. In FSW the most important area is stir zone, and these can be noted as a one of the differences between FSP and FSW processes. The second difference is that for FSP the important area is zone direct below pin, and for FSW is does not matter because basically the welding technology consist in joint throughout thickness of materials.

The main technological parameters of the FSP process are the following:

- rotational speed,
- travelling speed,
- tilt angle,
- penetration depth of the tool,
- kind of the tool (pin length, diameter and shape of the pin, diameter and shape of the shoulder).
- alloying material (SiC, $Al_2O_3$, etc.),
- cooling system,
- clamping system.

The detailed analysis of these parameters as well as prospective tools are presented in earlier publication [3].

The width of the processed zone by the single-pass FSP is slightly wider than the pin diameter. The traversing pattern may involve only a single linear or curvilinear processing pass as shown in Fig. 2a. Such a narrow processed zone might not be suitable for all practical engineering applications. Therefore, two approaches to increase the width of the processed zones are available [4]. The first one is to use a large diameter pin and the second one is to process the sample using multi-run FSP. In the first case the increase in the tool dimension causes the increase in the torque acting on the tool and this increases the demand for power of the machine. The second one with a certain level of overlap between the successive passes can guarantee the demanding properties of the modified material. Hence, it is important to understand the microstructure evolution during the multiple-pass FSP. The multi-pass techniques are illustrated in Fig. 2b–d. A wider surface of material can be subjected to the FSP thermomechanical cycle using a series of linear traverses, offset from one another by stepping over by a designed distance as presented in Fig. 2b. Due to tool rotation the deformation field near the tool pin is not symmetric to the axis of tool advance and therefore the variation in microstructure from the advancing side to the retreating side can be observed. Microstructure gradients are typically more pronounced on the advancing side than on the retreating side. A series of parallel traverses as suggested in Fig. 2b result in successive replacements of the advancing interfaces with retreating interfaces in the processed volume of material. In contrast, a raster pattern as shown in Fig. 2c results in a pattern of advancing/advancing and retreating/retreating interfaces in a direction transverse to the local direction of tool advance. Such a pattern may leave long-range gradients in microstructure in the stir zone and lead to strain localization with attendant low transverse ductility. The use of a spiral pattern such as that illustrated in Fig. 2d results in the replacement of the advancing interface with a retreating interface on successive passes and thus may mitigate gradients in stir zone microstructure. The step over distance is typically based on the pin diameter in order to assure overlap of stir zones on successive passes in multi-pass processing. As mentioned before, the stir zone is generally wider at the work piece surface due to the effect of the tool shoulder, and an excessive step over distance may result in incomplete overlap in lower regions of the stir zone on successive passes. Again, microstructure gradients within the stir zone may result in strain localization and reduced ductility. Using a step over distance that is ≈½ of the pin diameter at the mid-length of the pin generally eliminates such microstructure gradients [5].

Owing to its simple concept, various applications of FSP technology have been presented in the literature [6]. These include improvement in the corrosion resistance, mechanical properties, grain refinement in the microstructure, production of superplastic materials, reduction of the porosity of castings, or production of special alloys. Many different materials can be subjected the multi-run FSP technology, these include: cast and wrought aluminium alloys, copper, magnesium alloys, titanium and many others.

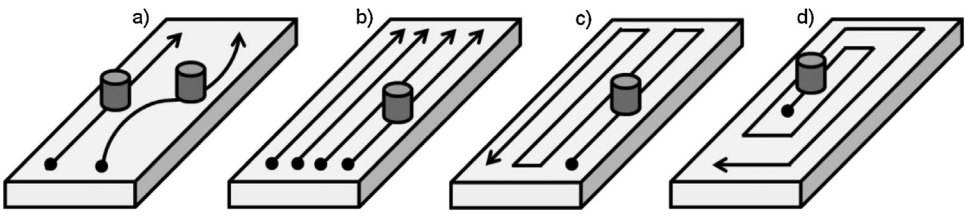


**Fig. 2 – Traversing patterns for FSP: (a) a single linear or curvilinear pass, (b) parallel passes offset by a step over distance, (c) raster pattern, and (d) spiral pattern [5].**

## 2. Torque, forces and heat in friction stir processing process

FSP is a relatively complicated process because the quality of surface of modified material depends on many parameters. Many phenomena observed in FSP are similar for that in FSW process. A fundamental understanding of relationship between technological parameters and torque and forces acting on the FSP tool is a principal issue to achieve the defect free modified materials [7].

In the FSP process the technological conditions can be divided into two groups: independent such as tool, workpiece, process parameters and machine and depended: forces and torque.

The most relevant loads acting on a machine during the FSP (FSW) process are the axial force ($F_z$), the traverse force ($F_x$), the side force ($F_y$), and the torque ($M$). The directions of these loads are displayed in Fig. 1.

The shoulder's dimensions, pin shape and diameter, material as well as tilt angle are tool parameters.

The workpiece – material – is also important, as the materials (melting point, physical and mechanical properties, chemical composition, thickness of modification – penetration depth) which could be modified by the FSP are limited.

Moreover, the rotational and travelling speeds as well as penetration depth are the main technological process parameters.

The above technological parameters have an impact on forces acting on the FSP tool as well as the quality of modified surface. Thus, to obtain a defect free modified area, the parameters should be selected properly for any types of base material [7–10].

In the FSP process, similar FSW, the tool due to its rotational and linear (curvilinear) movements, exerts axial and traverse forces on the modified material. These forces can lead to tool wear, deformation of modified element as well as clamping system. Therefore, prediction, monitoring and controlling these forces and torque are important. The knowledge of above phenomena makes it possible to [7]: optimize the tool design, predict tool wear, optimize clamping system, predict of the required clamp forces, obtain higher quality of the modified surface and select a suitable FSP (FSW) machine.

Various methods of measuring forces and torque acting on the FSP (FSW) tool can be applied. Generally speaking two groups of methods can be applied to measure axial and traverse forces as well as torque. Strain gauges, load cells and dynamometers techniques are types of direct measurement instruments. On the other hand, monitoring of current or power of the driver motor during FSP (FSW) process is indirect measurement methods [7].

Hattingha et al. [11] presented the measurement system, which is based on the strain gauges technique. When a bending moment is introduced on the tool during modification (or welding) the magnitude and direction of the resultant maximum and minimum forces can be detected during each tool revolution. Strain gauges allow traverse ($F_x$) and side ($F_y$) forces to be measured simultaneously. Four strain gauges can be mounted on the tool surface, 180° apart in a Wheatstone bridge configuration. Measurement of these signals during one full revolution produces a sinusoidal waveform. The dynamometer application in friction stir processes in [12–14] was presented. The friction stir machine was instrumented with a three-axis dynamic dynamometer. The forces were recorded along two main axes: parallel to the modified or welding line and perpendicular to the sheets. As a consequence, the system allows to measure $F_x$ and $F_z$ forces. The measuring of only axial force is also an useful solution for experimental analysis of the friction stir processes. A miniature button type load cell can be positioned inside the machine arbour in such a way that it is always in contact with the tool. The load cell wires are passed through a hollow draw bar to a rotating electrical connector (REC) at the top of the machine head, which operates similar to a slip ring. The Data Acquisition System equipped with LabView is connected to the REC with data cables [15]. To measure the torque, four torsional strain gauges can be also placed at the tool base 180° apart. The strain gauges and load cells can be embedded on the workpiece, by which the forces on the tool are indirectly being measured using this method. A typical friction stir system can be equipped with two load cells to measure both traverse and axial forces as well [16].

The second group of measuring method include inexpensive techniques which are based on measurements of the electrical parameters of drive motors. By means of reordered electrical signals, such as current, power, torque and proper calibration, these data allow forces and torque to be measured indirectly [17,18].

It should be noted, that the sophisticated friction stir machines are equipped with professional measurement systems [19]. The working heads have several sensors measuring the pressure inside the hydraulic actuators. The values of the forces $F_x$ and $F_y$, applied on the tool, are calculated from the measured momentum. The axial force $F_z$ and the spindle torque are calculated from the actuators placed into the spindle.

The FSP (FSW) can be carried out in specialized machines as well as typical milling machines. The first one are equipped with measurements system, while the second one need universal measurement head. Milling machines fail to provide the ideal conditions for FSP (FSW) processes. Since, the developing of independent measurement systems is an important issue. One option is a low cost friction stir monitoring unit – LOWSTIR. Four key elements of the unit can be identified; a measuring unit for recording forces and torques during the processes, a tool holder capable of removing heat from the tool to protect the measuring unit, tools appropriate to milling machine conditions and also software for capturing the required data and visualization of the important information. Fig. 3 shows the measurement unit [20,21].

It should be emphasized that the signals recorded during FSP (FSW) are characteristic for the specific tool geometry, parameters of the process, base material, measurement system (LOWSTIR) and experimental setup [22].

To gain the possibility to predict properties of the modified surface the relationship between process parameters (rotational speed, travelling speed, type of tool) – spindle torque – temperature – microstructure – mechanical properties – quality of stir zone need to be recognized.

**Fig. 3 – The Low stir measurement head.**

The total torque, which is the sum of the three components:

$$M_{total} = M_{shoulder} + M_{pin\_bottom} + M_{pin\_surface} \quad (1)$$

is related to the average power input by [25]:

$$Q_{total} = M_{total}\omega \quad (2)$$

where: $\omega$ – rotational speed [rpm].

During the FSP (FSW) process [23], heat is generated at or close to the contact surfaces, which have complex geometries depending on the tool geometry, but for the analytical estimation, a simplified tool design with a horizontal shoulder surface, a vertical cylindrical probe side surface and a horizontal (flat) pin tip surface is assumed. If $Q_1$ is the heat generated under the tool shoulder, $Q_2$ at the tool pin surface and $Q_3$ at the tool pin tip, hence the total heat generation, $Q_{total} = Q_1 + Q_2 + Q_3$.

Arora et al. [24] presented results on the relationship between parameters and $F_x$ force. They revealed that the increase in rotational speed, shoulder diameter and pin dimeter caused increase in the $F_x$ force, however, increase in the travelling speed caused decrease in this force. Also Trimble et al. [25] confirm that the increasing the travelling speed causes the increase in the torque, traverse and vertical forces.

The axial force is also influenced by travelling speed, rotational speed, tool shoulder and pin diameter [7]. The increase in travelling speed causes increase in $F_z$. This is an increase in the volume of stirred material per time unit. Moreover, the increasing of the rotational speed leads to increasing the temperature at the shoulder contact surface thus material is softening more easily and the decrease in $F_z$ can be observed [7,16].

However, the spindle torque is one of the main quantity parameter which decide about heat input, temperature in the stir zone, as well the safe load of clamping system and machine as well. Generally speaking the torque is the sum of sticking and sliding torques. With the increase in shoulder diameter the total torque increases continuously even when the sticking torque decreases for large shoulder diameters. In this regime, the extent of the decrease in the sticking torque is smaller than the increase in the sliding torque. As a result, the total torque increases continuously with shoulder diameter. These phenomena are observed for different rotational speeds [26].

The influence of the rotational and travelling speeds on the torque acting on the tool is shown in Fig. 4. The increase in this speed leads to a decrease in torque. This is caused by the fact that the increase in rotational speed of the tool causes an increase in temperature in surface between shoulder and modified material as well as in the stir zone. The friction coefficient becomes lower thus the material resistance decreases [27]. Simultaneously the modified material is liable to plastic deformation. The numerical modelling of these phenomena [28] revealed that two zones occurred in the friction stir area, that is a primary and a secondary zone. As the tool rotation speed increases, the diameter of the primary vortex zone decreases, and the process zone, itself, shows less tilt. With the increasing tool rotation speed, the concentration of streamlines within the secondary process zone also increases, indicating an increase in the coherency of this zone at the trailing edge of the tool.

However, the spindle torque is not significantly affected by the change in the travelling speed (Fig. 4b). The increase in torque with the increasing travelling speed at constant rotational speed [29] may be due to two contributing phenomena. Firstly, for a constant tool rotation speed and decreasing travelling speed, the volume of material being deformed on each revolution decreases, hence the heat is generated in a smaller volume, and this in turn may lead to slightly higher temperatures and lower flow stress. Secondly,

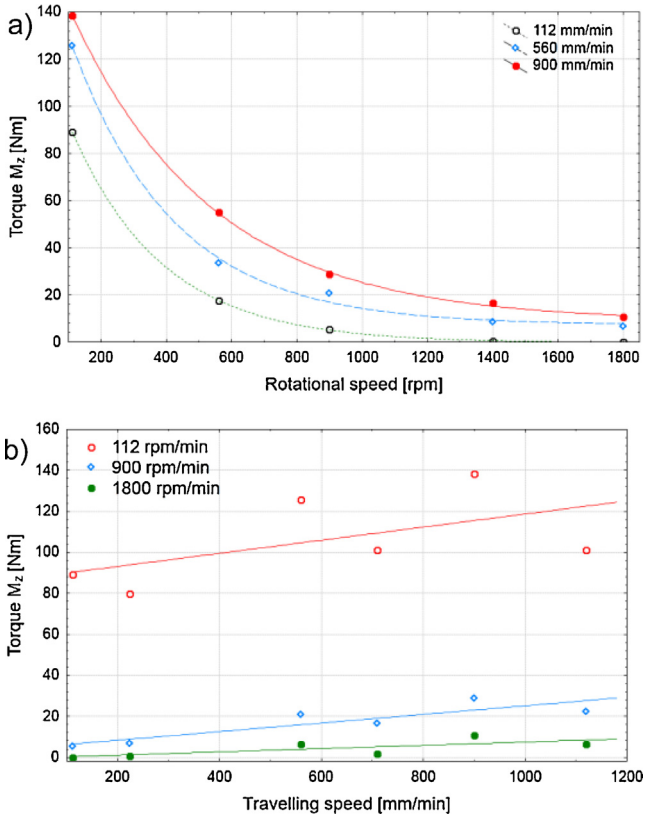


**Fig. 4 – Influence the (a) rotational speed and (b) travelling speed on the torque acting on the tool, aluminium alloy AlSi6Cu4, tool without pin.**

lower travelling speed will reduce the convective cooling, resulting from slower movement into the relatively cooler material in the front of the tool. The previous numerical modelling of the FSP process revealed [28] that, when the tool velocity increases, the primary process zone remains well developed, but the streamlines begin to ''lag behind'' the advancing tool causing the vortex to tilt from the leading edge towards the trailing edge into the workpiece thickness. At the same time, the diameter of the vortex has increased, indicating a loss in its degree of coherency. The secondary zone also remains clearly defined; however, the size of the secondary zone has decreased [30].

## 3. Microstructure refinement

The mechanical and physical properties of all crystalline metallic materials can be controlled and determined by several factors, such as: chemical composition, process of metallurgy as well as heat treatment. However, the average grain size of the material plays a significant role in many application. The strength of polycrystalline materials is related to the grain size, through the well knowing Hall–Petch equation – the strength increases with a reduction in the grain size [31]. This phenomenon leads to increasing interest in fabricating advance materials which can be characterized by ultra-fine grain (UFG) sizes, which are designed for specific applications [31]. Basically, three different grain size ranges can be distinguished: traditional ($d > 10^{-6}$ m), ultrafine-grain ($d$: from $10^{-8}$ to $10^{-6}$ m) and nanocrystalline ($d < 10^{-8}$ m) [32]. In order to convert a coarse-grained solid metal into a material with ultrafine grains or lower, it is necessary both to impose an exceptionally high strain in order to introduce a high density of dislocations and to subsequently re-arrange these dislocations to form an array of grain boundaries. In practice, conventional metal-working procedures, such as extrusion or rolling, are restricted in their ability to produce UFG structures for two important reasons. First, there is a limitation on the overall strains that may be imposed using these procedures because the processing techniques incorporate corresponding reductions in the cross-sectional dimensions of the workpieces. Second, the strains imposed in conventional processing are insufficient to introduce UFG structures because of the generally low workability of metallic alloys at ambient and relatively low temperatures. As a consequence of these limitations, attention has been devoted instead to the development of alternative processing techniques, based on the application of severe plastic deformation (SPD), where extremely high strains are imposed at relatively low temperatures without incurring any concomitant changes in the cross-sectional dimensions of the samples. For the SPD technologies a special machines are needed [31,33]. Many different SPD processing techniques have been proposed, developed and evaluated. These techniques include equal-channel angular pressing (ECAP), high-pressure torsion (HPT), multi-directional forging, twist extrusion, cyclic-extrusion–compression, reciprocating extrusion, repetitive corrugation and straightening (RCS), constrained groove pressing (CGP), cylinder covered compression (CCC), accumulative roll-bonding (ARB) and finally friction stir processing [31,33]. The average dimension of nanograins is in the range of 100–200 nm. Rather rarely the nanograin size is below 100 nm [33]. The innovation potential for these materials is growing and commercialization of UFG materials is now attracting much attention. The UFG materials will probably find major applications under extreme environmental conditions where the required properties are unusually severe (include biomedical applications, aeronautical systems, high-performance sports applications and for innovative developments in the energy, oil and gas sectors) [34].

Friction stir processing is one of the prospective technology which allows UFG materials to be fabricated. In FSP the final microstructure and consequent mechanical properties distribution are dependent on several independent factors. The main factors include chemical composition of modified material, temper conditions of delivery, technological process parameters, penetration depth (thickness of the modified area) and other geometric factors. Chemical composition determines the available strengthening mechanism and how the material will be affected by the temperature and strain history associated with FSP. The temper delivery state determines the preliminary microstructure of the parent material, which can has an important effect on the material response to FSP, particularly in the heat affected zone (HAZ). Process parameters such as rotational and travelling speeds determine, for established tool geometry and thermal boundary conditions, the temperature and strain history of the modified surface material. Plate gauge and other geometric factors particularly dimensions and shape of the tool, and heat sinks associated with clamping can influence on temperature distribution e.g. stir zone [35].

In FSP generated heat and deformation cause the parent material to flow at the temperature below melting point and allow traversing of the tool along designed modification line. The severe plastic deformation in the stir zone leads to a general change in microstructure [7]. To increase the forging action, the FSP tool is tilted approximately $\alpha = 1.5^{\circ}$ from the vertical position. Because the rotation of the tool and the forward motion are in the same direction on the advancing side, and on the retreating side the rotation motion and the forward motion are opposite the advancing side of the modified area is normally the hotter side of the process zone. Also higher stress level in the modified material can be observed for the advancing side than for the retreating side [36].

The heat is mainly produced by friction between the rotating shoulder and the workpiece, while the rotating pin deforms heated material locally. The heated material flows around the rotating pin and then fills the cavity at the rear of the tool. Hence, the FSP process can be assumed as a hot deformation technique and thus hot deformation microstructural mechanism can occur during FSP. The dynamic recrystallization mechanism occurred during FSP, which is responsible for production of new grains, can be divided into three types [7]:

- discontinuous dynamic recrystallization, occurs by nucleation and growth of new grains,
- continuous dynamic recrystallization, involves the formation of arrays of low angle boundaries and a gradual increase

in boundary misorientation during hot deformation, finally leading to new grain development,
– geometric dynamic recrystallization, resulting from the impingement of serrated grain boundaries, which can occur when grains are extremely elongated by severe hot deformation.

All of these mechanisms lead to grain refinement. The concepts of microstructure refinement, for aluminium alloy 5083, is shown in Fig. 5. The label description are presented below.

The aluminium alloy 5083 base metal in delivery condition is characterized by coarse grain microstructure – 1 in Fig. 5. Firstly, the material is subjected to SPD due to the extensive strain imposed by the rotating pin. The dynamic recovery (DRV) can be observed. The subgrain structure with high misorientation after their coalescence and rotation can be revealed – 2 in Fig. 5.

During FSP the temperature gradient occurred. Hence, the solutes come out of solution and precipitate due to a drop in temperature. This results in a transient in restoration mechanism when the DRV is interfered by the precipitation of second-phase particles resulting in the occurrence of continuous dynamic recrystallization (CDRX). The restoration by CDRX leads to a relatively fine and uniform grains through subgrain coalescence and rotation – 3 in Fig. 5. This is because the pinning of the grain boundaries, caused by the fine dispersion of the second-phase precipitates, occurs. Thus, during the CDRX, this phenomena can result in a stabilized subgrain structure. However, when deformation by FSP is almost over, the subsequent coarsening of the precipitates may lead to homogenous subgrain growth because the coarsened precipitates cannot pin the boundaries anymore. It should be noted that particles coarsening takes place in the heat affected (HAZ) zone not in the stir zone – 4 in Fig. 5.

The example macrostructure and microstructure of Al–Si alloy subjected to the FSP process are shown in Figs. 6 and 7b, respectively. Under a light microscope, α-Al phase appears bright while Si particles are dark. In the stir zone, as marked by the solid curve, the shoulder flow zone (upper region) and pin stir zone (below) can be identified. As shown, the stir zone displays a region of rotational shear material – RSM [38] on the

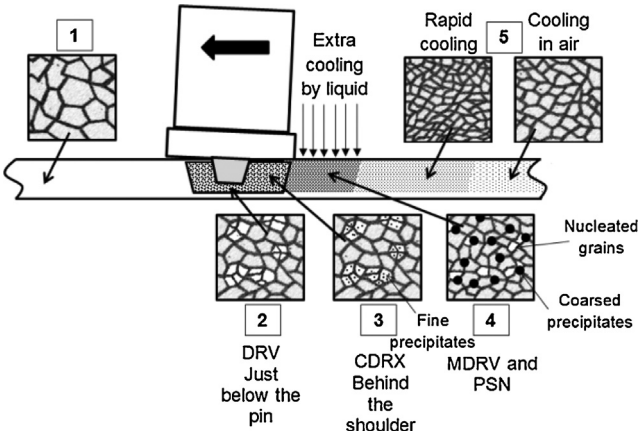


**Fig. 5 – Presented microstructural model for microstructural revolution during FSP, aluminium alloy 5083 [37].**

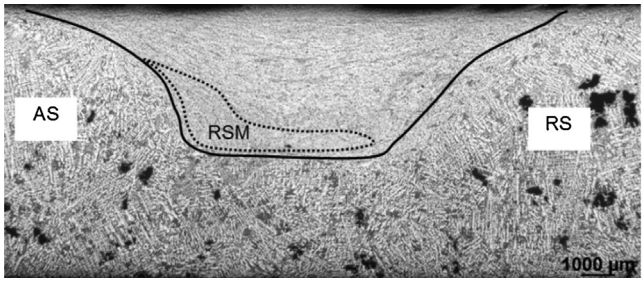


**Fig. 6 – Cross section of FSP area AlSi9Mg (advancing side on the left side).**

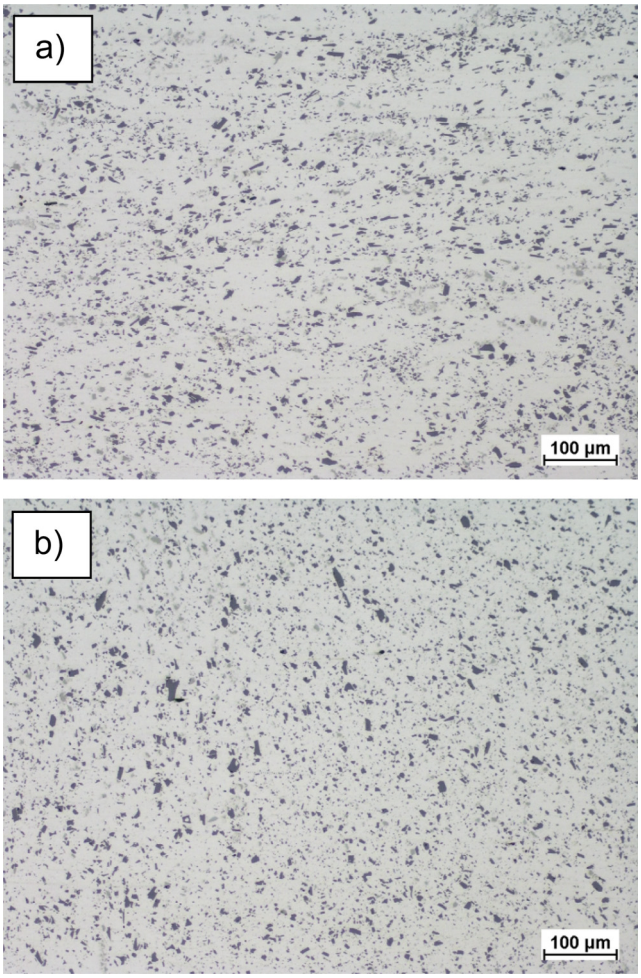


**Fig. 7 – Microstructure of stir zone area (a) for FSW welded joint and (b) FSP modified material, AlSi9Mg.**

advancing side (AS), extending but tailing off towards the retreating side (RS) in the mid-to-lower part of the zone. In the RSM region, Si particles have become quite evenly distributed in α-Al matrix. The rest of the stir zone (outside the RSM region) is material that has been deformed, but to a much lesser extent, particularly towards the RS. Thus, the Si particles originally concentrated in the interdendritic regions have remained, and the microstructure is still highly segregated. For the typical FSP technological condition $\omega = 560$ rpm, $v = 560$ mm/min, the RSM is quite low.

It should be noted, that base of the metallographic examination (light microscopy), there is lack of visible microstructure's differences of separated zones (advancing side, retreating side and stir zone) of material which undergoes FSW or FSP processes. The microstructure of advancing and retreating side of AlSi9Mg aluminium alloy (6 mm in thickness) are presented in Figs. 8 and 9, respectively. The FSW and FSP processes at the same technological parameters ($\omega$ = 560 rpm, $\upsilon$ = 560 rpm, Triflute tool) were carried out. The results indicated that the AS for both FSW welded joint and FSP modified material can be easily distinguished. Meanwhile, for RS the borders are smooth. Hardly, also any difference on the stir zones observed (Fig. 7). This is caused the fact that at the same materials and technological parameters (in the welded joint as well as modified material) material undergoes the same thermal and plastic deformation cycles.

However, the main difference in root areas can be observed. The pin length was lower than the plate thickness, thus the root is visible. For the welded joint the dark line separated the two joining plates is observed (Fig. 10a). The intense plastic deformation, forces acting on the welded plates and flow of material caused that the line takes the hook shape. For the FSP modified material there is a lack of this line (Fig. 10b).

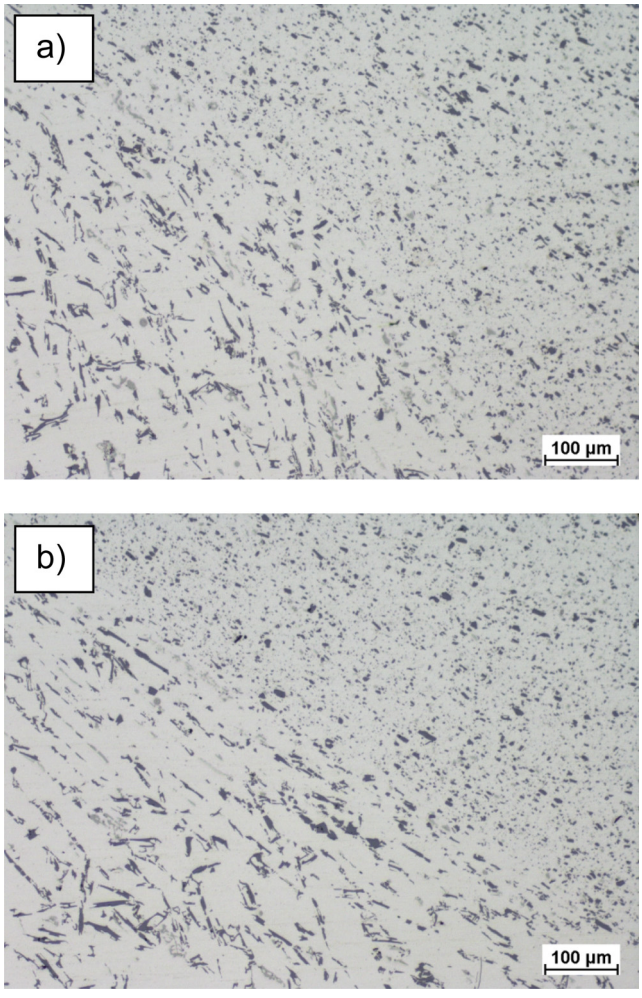


**Fig. 8 – Microstructure of advancing side area (a) for FSW welded joint and (b) FSP modified material, AlSi9Mg.**

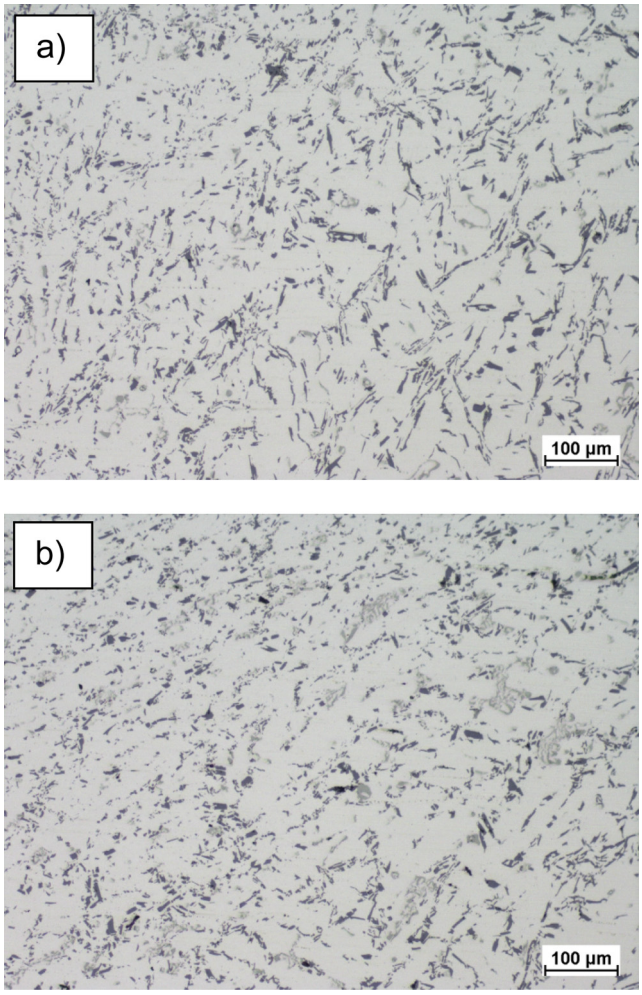


**Fig. 9 – Microstructure of retreating side area (a) for FSW welded joint and (b) FSP modified material, AlSi9Mg.**

To produce the UFG materials in FSP process standard techniques as well as special solutions can be used. The first group of methods is based on utilizing different kind of tool namely different tool materials, different pin shape as well as shoulder [39]. A proper range of modification parameters allows achieving UFG modification in a wide range of parent metals. However, as mentioned before the addition of cooling procedure allows the reduction of the grain size increase. In order to obtain rapid heat sink during FSP, an efficient cooling system should be designed. To transfer the heat generated by the samples from FSP quickly, it is necessary to shorten the barrier between the samples and the liquid coolant (e.g. nitrogen). So two tunnels can be machined beneath the surface for the copper mould, where the liquid nitrogen could immerge [40]. The plate, during FSP, can be also completely submerged in liquid coolant e.g. water, and this novel FSP technique is called submerged FSP. During the submerged FSP, flowing water is also used to quench the plate immediately behind the FSP tool in order to further inhibit the growth of the recrystallized grains [41]. Another useful methods are multi-pass techniques. With the increase in number of passes, the grain size decreases gradually with a corresponding decrease in free dislocation density. The grain size decreases upon the

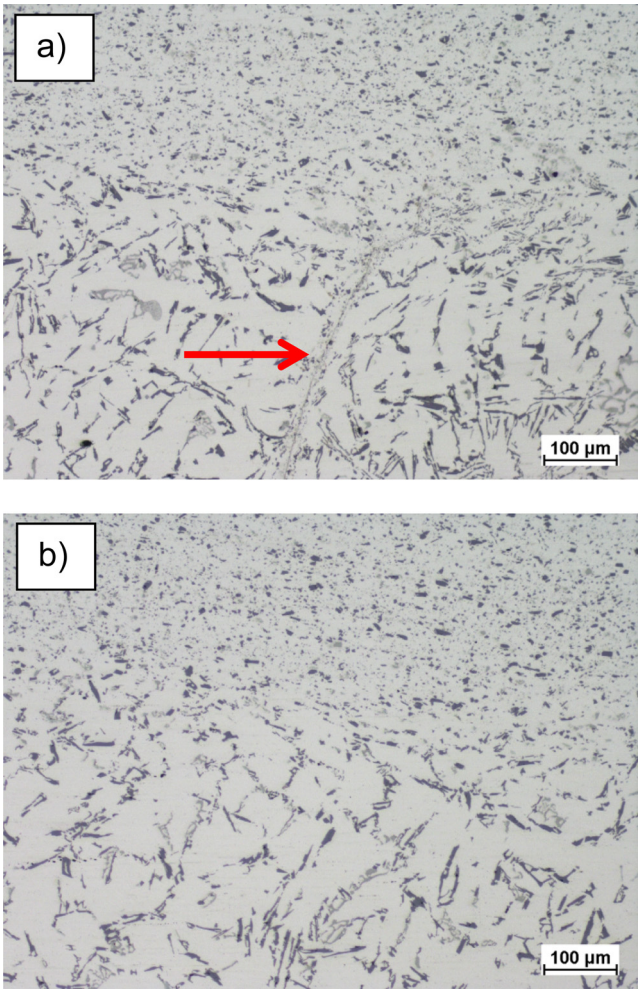


**Fig. 10 – Microstructure of root area (a) for FSW welded joint and (b) FSP modified material, AlSi9Mg.**

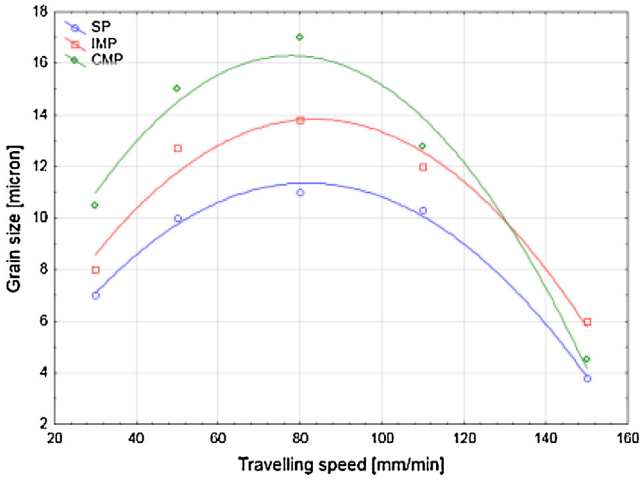


**Fig. 11 – Variation in grain size with traverse speeds for different FSP conditions. SP – single pass, IMP – intermittent multipass, and CMP – continuous multipass [43].**

first pass; but, subsequently, no significant changes are observed up to six pass of FSP [42].

The sequence of the multipass technique can also decide about a grain size. Ramesh et al. [43] presented the result of a single pass (SP) as well as multipass for different thermal history. The Authors presents intermittent multipass FSP (IMP) technique in which the material was allowed to cool back to room temperature after each pass of FSP and then the subsequent pass was carried out. The second technique was continuous multipass FSP (CMP) process in which the FSP was continuously performed for 12 passes without allowing any cooling time between passes. SP, IMP and CMP processing have different effects on microstructural evolution, which may be attributed to different thermal cycle. Fig. 11 shows effect of travelling speed on a grain size in the nugget zone after SP, IMP, CMP. The grain size is found to increase with a travelling speed of up to 80 mm/min and then starts decreasing at a higher speed. The pattern of variation in a grain size is similar under all variants of processing. Up to the travelling speed of 110 mm/min, the grain size obtained after CMP is coarser than in IMP and single-pass processing. However, after processing using a travelling speed of 150 mm/min, the grain size obtained for all the processing variants lies within a narrow range. This is because of an effect of thermal cycle on the microstructure after multipass using IMP and CMP variants [43].

Multi-run friction stir processing can be carried out in parallel runs (Fig. 2). In such way the adjacent beads overlapping each other in the wide range can be performed. The second option is that the second run perpendicularly to the first one can be carried out [44]. The modified area resulted in the refinement of the microstructure. As a result of FSP the as-cast material is converted into a near-wrought condition. The other feature revealed by TEM was the presence of a large number of subboundaries as well as a fairly high dislocation density introduced into the processed material. Since aluminium has a high stacking fault energy, the dislocations are tangled rather than confined to their slip planes. The presence of dislocations suggests that recrystallization is not complete and that it have a more dynamic nature than static character. In addition, the microstructure consists of small subgrains, confirming intense dynamic recovery occurring during FSP. The TEM analysis revealed that the dislocation density is higher for perpendicular runs technique than for material achieved at parallel runs [44].

Weglowski et al. [44] revealed, that the friction stir processing treatment resulted in significant increase in the elongation up to 12.5%. The UTS increased to 216 MPa (increase of 42%), however, the YS decreased to 117 MPa. The lowering of the YS as a result of FSP may be attributed to the presents of free mobile dislocation ready to take part in the deformation process just after an application of stress. The lowering of the YS and simultaneous increasing of the UTS indicate a strong dislocation hardening effect during deformation. Leal et al. [39] present results about improvement in the electrical conductivity of the processed material. The FSP of steel caused higher resistance to cavitation erosion in comparison to un-processed steel [46]. The examples of utilization of FSP for grain refinement are given in Table 1.

**Table 1 – Examples of utilization of FSP for grain refinement.**

| Parent material | Average grain size Parent material/FSP | Ref. |
|---|---|---|
| Steel 13Cr4Ni | 25 μm/0.6 μm | [46] |
| AZ31 | 75 μm/100 nm | [47] |
| Al-4Mg-0.8Sc-0.08Zr | 19 μm/0.49 μm | [48] |
| 1050 | –/0.5 μm | [45] |
| Al-7Si-0.3Mg | 188 μm/1.3 μm | [42] |
| C12200 H02 | 18 μm/0.5 μm | [39] |
| AZ61 | 75 μm/100 nm | [40] |
| Cu | –/800 nm | [49] |
| AlSi9Mg | /200 nm to 1 μm | [50] |
| 5086 | 48 μm/6 μm | [43] |
| AZ91 | 150 μm/4 μm | [51] |
| WE43 | 35 μm/2 μm | [52] |
| Mg–Li–Al–Zn | 5–100 μm/1.6 μm | [41] |
| Steel D2 | 40 μm/1.6 μm | [53] |
| A356 | –/2 μm | [44] |
| Ti-6Al-4V | 500 μm/1 μm | [54] |

## 4. Friction stir alloying

The FSP process can also be used with a consumable material. It is then referred to as friction stir alloying – FSA (mechanical alloying). The examples of the combination of base material – consumable material used in FSA procedure are presented in Table 2.

The surface properties such as wear and corrosion resistance, hardness, strength, ductility, fatigue life and formability without affecting the substrate properties can be improved by using FSA. Basically, FSA is used for producing surface composites in aluminium and magnesium alloys both is cast as well as wrought delivery condition. However, the latest development of FSA tool investigation have revealed that surface composites of high melting point materials including cupper, steel and titanium based alloys can also be produced. FSA allows fabrication of all variants of surface composites with limited interfacial reaction with the reinforcement material. The consumable material can be applied as powder, wire or plate. The most common methods for placing reinforced consumable in the fabrication of surface composites by groove, drilled holes or using cover plate are presented in Fig. 12.

The following steps based on the groove method with reinforcement particles are presented in Fig. 12a. Firstly, the proper groove in relation of dimensions is machined on the modified substrate and the reinforcement particles are filled in the groove. Next, FSP tool without a pin closes the groove completely. In the last step, the FSP tool with a pin is applied on the closed groove fulfilled consumable. The dimension (width and depth), shape (rectangular, triangular, oval, etc.), number of grooves, distance between each other can be varied to achieve required volume fraction of the reinforcement particles [86].

**Table 2 – Example of material combination used in FSA technology.**

| Base mat. | Consumable | Powder size | Ref. |
|---|---|---|---|
| AZ61 | $SiO_2$ | 20 nm | [55] |
| AZ31 | $C_{60}$ | – | [56] |
| AZ31 | SiC | 1 μm | [57,58] |
| AZ91 | SiC | 5 μm | [59] |
| AZ31 | $Al_2O_3$ | 35 nm, 350 nm, | [60] |
| AZ91 | $Al_2O_3$ | 30, 300 nm | [61] |
| AZ31 | $SiO_2$ | 10 nm | [62] |
| A413 | Ni | 3 μm | [63] |
| 7075 | C NT | – | [64] |
| 1100 | $TiO_2$, $SiO_2$ | 0.7 μm, 17 μm | [65] |
| | SiC | 0.7 μm | [66] |
| 1050 | SiC | 1.25 μm | [67,68] |
| A356 | SiC | 30 μm | [69] |
| A356 | $MoS_2$ | 5 μm | [69] |
| 5052 | SiC | 50 nm, 5 μm | [70] |
| 1050 | SiC + $Al_2O_3$ | 1.25 μm | [71] |
| 6360 | TiC + $B_4C$ | 3 μm | [72] |
| 5083 | SiC, $MoS_2$ | 5 μm | [73] |
| 2024 | $Al_2O_3$ | 50 nm | [74] |
| 6082 | $Al_2O_3$ | 50 nm | [75] |
| 5083 | Cu | 20 μm, 40 nm | [76] |
| Cu | SiC | 5 μm | [77,78] |
| Cu | $B_4C$ | 4 μm | [79] |
| HDPA | Nanoclay | | [80] |
| Steel | TiC | 70 nm | [81] |
| Steel | $Al_2O_3$ | 70 nm | [82] |
| Ti | SiC | 50 nm | [83] |
| Ti | N | – | [84] |
| Ti | $Al_2O_3$ | 20–80 nm | [85] |

The groove methods are applied for in a lot of research to fabricate surface composites such as: 5083/Cu [76], Ti/$Al_2O_3$ [85], 5083/SiC and $MoS_2$ [75] and many others.

The second method of fabricating the surface composite material is a drilled-hole method (Fig. 12b). Numerous blind-holes as the reservoirs for reinforcement particles can be prepared on the substrate plate surface via automatically mechanical drilling methods. The holes could be arranged according to desired geometry. The hole depth, diameter as well as arrangement of each other decide about total volume of reinforcement particles in composite surface [86].

To avoid the ejection of reinforcement particles from the groove or drilled holes the thin sheet as a cover can be applied

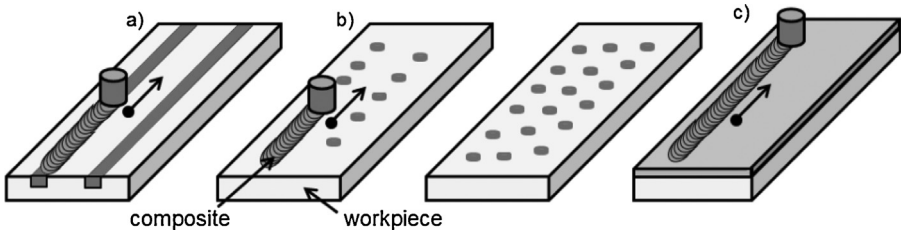


**Fig. 12 – Common methods for placing reinforced particles in the fabrication of surface composites (a) by a groove, (b) by a drilled holes and (c) by using cover plate.**

(Fig. 12c). This technique was adopted to produce nanotubes reinforced with 7075 aluminium alloy [87] and, in Cu plate reinforced with $Y_2O_3$ particles [88]. The new concept is based on the Direct Friction Stir Processing (DFSP) [89]. In this method a hollow and the tool without a pin to fabricate the surface composite are used. The reinforcement particles flow out through the through-hole of FSP\FSA tool and enter the enclosed space between a shoulder and substrate metal. They are then pressed into the workpiece. The another option is to use a consumable tool with holes filled with reinforcement material [90]. One of the more prospective method for fabrication of the surface composite is using FSP process on composite coating prepared by the use of thermal spraying such as plasma [74] or high velocity oxy-fuel (HVOF) spraying [102]. A novel approach involved air plasma spraying of Al–10% $Al_2O_3$ powder to produce Al–10%$Al_2O_3$ coating on substrate. The coated material was then subjected to friction stir processing (FSP) to distribute $Al_2O_3$ particles into the substrate [74]. At the second option the composite powders (A356–5vol.% $Al_2O_3$ composition) were deposited onto the grit blasted A356-T6 substrates by HVOF spraying [91]. Then plates with preplaced composite coatings were subjected to FSP. Friction Stir Processing can be also used effectively to homogenize the particle distribution in Al based in situ composites [92]. An Al–5 wt.% TiC composite was processed in situ using a mixture of K2TiF6 and graphite powders in aluminium melt. FSP was employed on the as-cast composite to uniformly distribute the TiC particles in the Al matrix. The composite was subjected to single and double pass FSP. A combination of FSP and electrophoretic deposition is also possible. The Authors [93] revealed that fabrication of nano-hydroxyapatite coatings on the Ti-CaP nanocomposite surface layer is a promising technology. The combination of FSP and subsequent rolling processing allows carbon nanotube (CNT)-reinforced 2009Al composites to be fabricated. Submerged friction stir processing under cryogenic conditions to fabricate ultrafine-grained nanocomposites with enhanced mechanical characteristics can also be applied [94]. Reactive friction stir processing by blowing nitrogen gas into the stir zone can be applied to manufacturing the composite surface as well [83]. The mixture of different reinforcement particles (powders) is also a prospective method of increasing hardness as well as improving wear resistance [73]. Fig. 13 shows the relationship between weight loss and the sliding distance of as-cast A356 and as-processed samples. As can be seen, the wear weight loss increases with sliding distance.

For the surface hybrid composite, the wear weight loss is the lowest among of test samples under the wear test condition [69]. Like the FSP without consumable material also the FSA is dependent on technological parameters. Type of material substrate: melting point, yield strength, hardness, chemical composition, rotation tool speed and travelling speed will determine the efficiency of the FSA.

The multi-pass FSA method using the consistent process parameters could be employed to obtain a large scaled processed zone [95]. Multi-pass FSP also leads to a reduction in size of cluster and uniform distribution of reinforcement particles and thus decreases the grain size of matrix. In friction stir processed surface composite, the reinforcement particle distribution mainly depends on number of FSP passes [62,96].

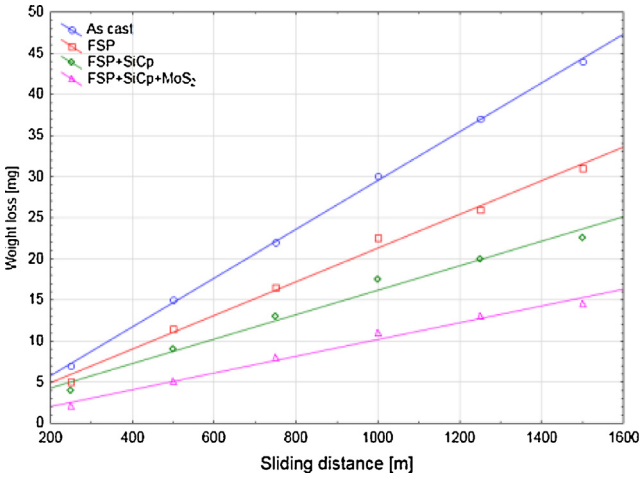


**Fig. 13 – Variation of weight loss with the sliding distance [69].**

The microstructure of modified area varies significantly with rotational and travelling speeds. The slow travelling speed rate causes greater heat input; hence it significantly changes the microstructure beneath the surface where extremely small grains are evident. The microstructure is very homogenous, with the large precipitates and defects partly broken. Intense plastic deformation and heat input during FSP cause the break-up of coarse dendrites and second-phase particles, the refinement of matrix grains, the closure of porosity, and the dissolution of precipitates, thereby creating a fine, uniform, and defect free structure [97]. However, high rotational speed affects grain refinement due to high heat input [60]. Thus, rotational and traverse speed must be optimized to achieve a defect-free SZ and reduced grain size. Kurt et al. [97] showed that increasing rotating tool speed and travelling speed caused a more uniform distribution of SiC particles in AA1050 alloy surface composite.

One of the most important factor in FSA technology is tool geometry as well as wear resistance. The most popular are threaded cylindrical, square and triangular pin profiles. The surfaces of the pin can also have different shapes and features including threads, flats or flutes. Thread-less pins are suitable for processing of harder alloys or metal matrix composites as the threaded features can be easily worn away. On the other hand tool wear is the most critical issue in the fabrication of surface composites due to especially hard reinforcement particles. Tool materials generally used for light alloys are various tool steels like H13 steel, whereas tungsten based alloys, cermetal (WC-Co) and poly cubic boron nitride (PCBN) are used for FSA of harder materials. Some other special tool materials including iridium-rhenium (Ir-Re), tungsten-rhenium (W-Re), cobalt (Co) alloys and tungsten carbide (WC) are also successfully employed. PCBN is preferred friction stir tool material for hard alloys such as copper, steels and titanium alloys due to its high mechanical and thermal performance. However, high cost and low fracture toughness of PCBN require immediate attention to develop cost effective and durable tools [98]. The reducing tool wear by cooling during FSP/FSA can be achieved, for example using gas injection direct on the FSP/FSA tool.

## 5. Friction stir processing with ultrasonic vibration

Friction stir processing with ultrasonic vibration is one of the prospective technologies which enable further refinement of the microstructure as well as improve the mechanical properties is.

Many different terms are available to refer the above new variants of FSP/FSW technologies. Linking terms such as "assisted" or "enhanced", or "modified" are frequently used to bridge the FSP/FSW process and the energy complementing the process. "Hybrid FSW" would be a reasonable term; however, this terminology is already in use to refer to the application of FSW to repair fusion welds [99,100]. In this paper, the term "assisted" is applied.

It should be noted that the ultrasonic energy for conventional manufacturing processes, such as: forming, machining, and welding has been used for years. The earlier results indicate that applying ultrasonic energy to a tool and/or workpiece in various metal-forming processes affects those processes in such a way that: process forces can be reduced, processing speeds can be increased, and product quality is improved [101]. These are due to superposition and local heating which occur when oscillatory energy is applied during the plastic deformation of metals. In most studies, superposition has been considered to be the major mechanism responsible for the reduction in forming force. The static force reduction during forming was found to be equal to the periodic force amplitude induced in the workpiece. Moreover, the results revealed that ultrasonic vibration decreased the yield stress and flow stress of the metal during plastic deformation [100].

Rusinko [102] revealed that the ultrasonic waves stimulate the blocked dislocations, hardened under ordinary deformation and decrease stresses for further plastic deformation. The validation of this observation was confirmed both by the finite element modelling and experimental trials [103]. The ultrasonic energy has the similar effect as thermal softening. However, the experimental results reveal that the ultrasonic energy, required to produce an identical level of softening, is $10^7$ times lower than the required thermal energy. This is caused by the fact that the ultrasonic energy is mainly absorbed at the dislocations in grains and is hardly absorbed in the defect free zones of the crystal, whereas the heat energy is distributed rather uniformly throughout the material by conduction [100]. Thus, the implementation of ultrasonic energy to assist the FSP/FSW process can be useful.

Integration of the ultrasonic system with FSP/FSW machine is easy. The ultrasonic energy source can be independently designed and system is based on four components as follows [100]:

a) the ultrasonic generator – which generates a high frequency electrical sinusoidal wave/alternating voltage with a specific frequency (generally 20 kHz, optimum 40 kHz) from a supplied power source,
b) the piezoelectric converter/transducer – which transforms the sinusoidal wave into mechanical oscillations of the same frequency. The wave has a low amplitude,
c) the booster/amplifier – which amplifies the oscillation amplitude/vibrational energy as suitable to the application; the amplitude is generally in the range of 5–50 mm,
d) the sonotrode or ultrasonic horn that transmits the vibrational energy into the workpiece.

Various transmission techniques of ultrasonic energy into the workpiece can be applied [100,104]. The ultrasonic energy can be transmitted onto workpiece from horn through FSP/FSW tool via bearing (horizontal direction to the tool), through tool (along the axial direction to the tool), directly on far end of one of the workpieces and directly into the stir zone (Fig. 14).

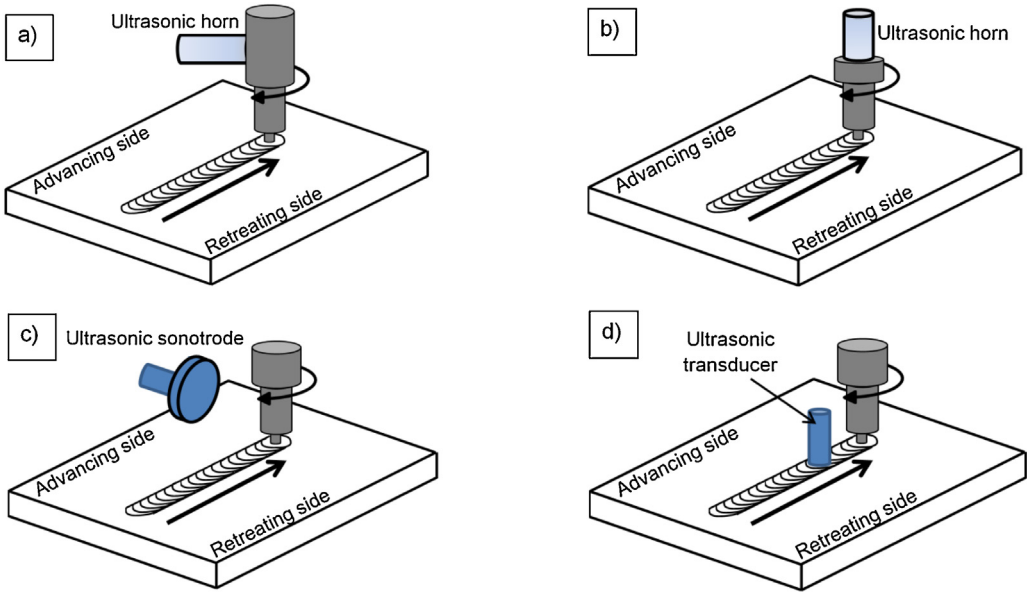


**Fig. 14 – Diagrams of ultrasonic assisted FSP/FSW techniques where ultrasonic energy is transmitted (a) onto workpiece from horn a through FSW tool via bearing, (b) through tool, (c) directly on far end of one of the workpieces, and (d) directly into stir zone.**

It should be notice, that no matter which system is used, the horn have to be precisely designed so that the resonance frequency of the horn matches the working frequency of the ultrasonic generator. The ultrasonic energy transmission efficiency of the horn increases with the reduction in the area of contact between the horn and the energy recipient stir zone [100].

Park et al. [101] applied ultrasonic vibrations on the FSW tool in horizontal direction via bearings during the FSW process and studied the effect of vibrations on the process at different process parameters. They revealed that reduction in axial force ($F_z$), to compare to conventional FSW process, is possible. The reduction of the axial force by increasing the ultrasonic vibration amplitude can also be achieved. The trends of variation was similar for the traverse force but the percentage of reduction is lower as compared to that of the axial force. A subsequent FEM analysis supported aforementioned observations. It should be noted, that by using ultrasonic vibrations assisted technique, defects are reduced and mechanical properties of the welding zones can be improved [104].

The advantage of ultrasonic vibrations system exerted in axial direction to FSW tool is that it is easily integrated without use of any bearings, allowing direct transfer of vibrations in the desired location. Ruilin et al. [105] revealed that application of such type of ultrasonic system is less effective for the temperature field while working at lower welding speeds. This was attributed to the additional heat input generated by the ultrasonic vibration in the UaFSW (ultrasonic assisted FSW) model. At lower welding speeds, the maximum temperatures of both FSW and UaFSW were identical but at higher welding speeds, decrease in the maximum temperature is grater in FSW than in UaFSW. Their numerical simulations showed a relatively larger welding process window with UaFSW. Moreover, Ma et al. [106] observed that the mechanical properties such as tensile strength, hardness and weld elongation of welds in UaFSW improved when the supply of ultrasonic energy was 50%, however, the hardness and tensile strength were in a state of decline when the ultrasonic energy reached more than 50%.

Strass et al. [107] applied ultrasonic vibration parallel to the welding direction either through the workpiece directly or through the backing plate (Fig. 14c). In this system, the intended stir zone is far away from the zone of energy transfer. Strass et al. applied this system in the dissimilar welding of AA5454/AZ91 alloys. The results revealed that the tensile strength of the welded joint increased by about 30%, and the brittle intermetallic layers were eliminated.

The ultrasonic vibration can be also directly and dynamically transmitted along the welded joint of the workpieces just ahead of the FSW tool by the sonotrode during welding (UVeFSW). Liu et al. [108] revealed that the improved weld physical and mechanical properties in the UVeFSW process is due to increased material deformation and reduced heat affected zone, respectively. Moreover, the ultrasonic vibration enhances the material flow, deformation in the weld nugget zone and widens the thermo-mechanically affected zone.

The ultrasonic assisted friction stir processes have been in their preliminary stages of development, and the studies available in the open literature are limited and basically covered the FSW processes. The details of the selected process conditions of different studies found in the literature are given in Table 3.

The main objective of the assistant energy fields is to reinforce material plasticization either directly or by generating additional heat in the FSW/FSP processes [104]. Thus, the prospective results of ultrasonic vibration assisted in FSW process tend towards research with the view the FSP processes can be also supported by the ultrasonic systems.

Zinati [109] presented the results of modified method of friction stir process combined with ultrasonic vibrations (onto workpiece from horn a through FSW tool via bearing) in order to reinforce polyamide 6 (PA 6) using multi-walled carbon nanotubes (MWCNT). MWCNTs have a diameter of about 15–30 mm and length of several micrometres. The results revealed that an increase in travelling speed leads to an increase of the stir intensified by the energy imposed by ultrasonic vibrations. Simultaneously, energy imposed by ultrasonic vibrations accelerates nano-composite fabrication process without affecting dispersion, homogeneity, and hardness. Therefore, nano-composite material can be fabricated at higher travelling speed without reduction of stirring during FSP.

Kumart [110] presented the results of comparative study of FSP and UaFSP on AA 6063 at different sets of rotational and travelling speeds. Tensile strength, surface roughness, micro hardness, temperature profiles, axial and transverse forces are compared for both FSP and UaFSP processes. The ultrasonic vibrations were applied along processing direction and perpendicular to the FSP tool. The ultrasonic generator allowed achieving the frequency in frequency range of 19–21 kHz. Theoretical amplitude of 12 mm was obtained as vibration amplitude at horn tip for UaFSP experiments. Plate of 6063 aluminium alloy (6 mm in thickness) was used for performing the experiments of FSP and UaFSP. The results revealed that at 70% and 90% of ultrasonic power FSP process enabled obtaining better mechanical properties than that of at

**Table 3 – Materials, process parameters employed in reported ultrasonic assisted FSW processes [100].**

| Workpiece | Rotational speed rpm | Welding speed mm/min | Ultrasonic characteristics |
|---|---|---|---|
| 6061-T6 | – | – | 20 kHz, 40 μm, 300 W |
| 6061-T651 | 1500, 1800 | 25, 50 | 40 kHz, 5–50 μm |
| 6061-T6 | 500, 710, 1000 | 64, 100, 142 | 20 kHz |
| 5454/AZ91D | – | – | – |
| 2024 | 600 | 800 | 20 kHz, 40 μm, 300 W |
| 6061-T6 | 350–1400 | 40–100 | 20 kHz, 40 μm |
| 6061 | 800, 1000, 1200 | 40, 70, 100 | 28 kHz, 12 μm |

80% and 100%. The values of yield strength, ultimate tensile strength and elongation of specimens produced with ultrasonic assisted technique are higher in most of the cases as compared to traditional FSP process. Moreover, a decrease in axial force by using ultrasonic vibrations as compared to conventional FSP can be observed. The peak temperature is also higher in case of ultrasonic vibrations as compared to conventional FSP process. It has shown that ultrasonic vibrations impart heat to the FSP region, causing the peak temperature rise.

## 6. Summary

FSP technology is a good example of the joining technology (FSW), which can be used for after some modifications for other purposes. It should be noted, however, that the friction stir processing technology is still not known solution, especially from the viewpoint of practical use in the industrial environments. Scientific studies carried out on laboratory scale have shown that microstructure and its associated physical and mechanical properties of the modified materials may be attractive, and the same technology can be competitive with currently used solutions. As well know, some solutions are no longer protected by patent protection, and therefore the investment costs which must be borne by investors in the implementation of technology FSP become lower. The chapter presents the ideas of the method, the role of the basic parameters and only some possibilities offered by FSP technology in terms of modifying the surface. Other areas of interest include scientists increase the plasticity of materials, modification of welded joints, production of composite materials, repair of casting elements and many others. FSP is a green technology – no welding fumes and dusts, there is no need to employ highly qualified welders, only equipment operators. Hence, it can be assumed that in the next few years, this technology will become increasingly important and will compete with traditional surfacing technologies.

## REFERENCES


[1] W.M. Thomas, E.D. Nicholas, et al., GB Patent Application No. 9125978.8, 1991.
[2] R.S. Mishra, Friction stir welding and processing, Materials Science and Engineering Reports 50 (2005) 1–78.
[3] R.M. Miranda, J. Gandra, P. Vilaça, Surface modification by friction based processes, in: Modern Surface Engineering Treatments, InTech, 2013.
[4] Z.Y. Ma, S.R. Sharma, R.S. Mishra, Effect of multiple-pass friction stir processing on microstructure and tensile properties of a cast aluminum–silicon alloy, Scripta Materialia 54 (2006) 1623–1626.
[5] T.R. McNelley, Friction stir processing: refining microstructures and improving properties, Revista de Metalurgia 46 (2010) 149–156.
[6] Z.Y. Ma, Friction stir processing technology – a review, Metallurgical and Materials Transactions A 39 (2008) 642–658.
[7] M.K.B. Givi, P. Asadi, Advances in Friction Stir Welding and Processing, Woodhead Publishing, Amsterdam, 2014.
[8] N. Mendes, P. Neto, A. Loureiro, et al., Machines and control systems for friction stir welding: a review, Materials and Design 910 (2016) 256–265.
[9] C. Hamilton, M.St. Węglowski, S. Dymek, P. Sedek, Using a coupled thermal/material flow model to predict residual stress in friction stir processed AlMg9Si, Journal of Materials Engineering and Performance 24 (2015) 1305–1312.
[10] M.St. Węglowski, Friction stir processing technology – new opportunities, Welding International 28 (2014) 583–592.
[11] D.G. Hattingha, C. Blignaulta, et al., Characterization of the influences of FSW tool geometry on welding forces and weld tensile strength using an instrumented tool, Journal of Materials Processing Technology 203 (2008) 46–57.
[12] A. Astarita, A. Squillace, L. Carrino, Experimental study of the forces acting on the tool in the friction-stir welding of AA 2024 T3 sheets, Journal of Materials Engineering and Performance 23 (2014) 3754–3761.
[13] R. Moshwan, F. Yusof, et al., Effect of tool rotational speed on force generation, microstructure and mechanical properties of friction stir welded Al–Mg–Cr–Mn (AA 5052-O) alloy, Materials and Design 66 (2015) 118–128.
[14] C. Jonckheere, B. de Meester, et al., Torque, temperature and hardening precipitation evolution in dissimilar friction stir welds between 6061-T6 and 2014-T6 aluminum alloys, Journal of Materials Processing Technology 213 (2013) 826–837.
[15] S. Mandal, J. Rice, A.A. Elmustafa, Experimental and numerical investigation of the plunge stage in friction stir welding, Journal of Materials Processing Technology 203 (2008) 411–419.
[16] R. Kumar, K. Singh, S. Pandey, Process forces and heat input as function of process parameters in AA5083 friction stir welds, Transactions of Nonferrous Metals Society of China 22 (2012) 288–298.
[17] H. Su, C.S. Wu, S. Pittner, M. Rethmeier, Simultaneous measurement of tool torque, traverse force and axial force in friction stir welding, Journal of Manufacturing Processes 15 (2013) 495–500.
[18] M. Mehta, K. Chatterjee, A. De, Monitoring torque and traverse force in friction stir welding from input electrical signatures of driving motors, Science and Technology of Welding and Joining 18 (2013) 191–197.
[19] S. Zimmer, L. Langlois, J. Laye, R. Bigot, Experimental investigation of the influence of the FSW plunge processing parameters on the maximum generated force and torque, The International Journal of Advanced Manufacturing Technology 47 (2010) 201–215.
[20] CORDIS EU, http://cordis.europa.eu/publication/rcn/12817_en.html.
[21] S. Cui, Z.W. Chen, J.D. Robson, A model relating tool torque and its associated power and specific energy to rotation and forward speeds during friction stir welding/processing, The International Journal of Machine Tools and Manufacture 50 (2010) 1023–1030.
[22] M.St. Weglowski, A. Pietras, Friction stir processing – analysis of the process, Archives of Metallurgy and Materials 56 (2011) 779–788.
[23] H. Schmidt, J. Hattel, J. Wert, An analytical model for the heat generation in friction stir welding, Modelling and Simulation in Materials Science and Engineering 12 (2004) 143–157.
[24] K.S. Arora, et al., Effect of process parameters on friction stir welding of aluminum alloy 2219-T87, The International Journal of Advanced Manufacturing Technology 50 (2010) 941–952.
[25] D. Trimble, J. Monaghan, et al., Force generation during friction stir welding of AA2024-T3, CIRP Annals – Manufacturing Technology 61 (2012) 9–12.

[26] A. Arora, A. De, T. DebRoy, Toward optimum friction stir welding tool shoulder diameter, Scripta Materialia 64 (2011) 9–12.
[27] J.T. Khairuddin, J. Abdullah, et al., Principles and thermo-mechanical model of friction stir welding, in: R. Kovacevic (Ed.), Welding Processes, 2012.
[28] C. Hamilton, M.St. Węglowski, S. Dymek, A simulation of friction stir processing for temperature and material flow, Metallurgical and Materials Transactions B 46 (2015) 1409–1418.
[29] A. Arora, R. Nandan, A.P. Reynolds, T. DebRoy, Torque, power requirement and stir zone geometry in friction stir welding through modelling and experiments, Scripta Materialia 60 (2009) 13–16.
[30] M.S.T. Węglowski, S. Dymek, Microstructural modification of cast aluminium alloy AlSi9Mg via friction modified processing, Archives of Metallurgy and Materials 57 (2012) 71–78.
[31] R.Z. Valiev, T.G. Langdon, Principles of equal-channel angular pressing as a processing tool for grain refinement, Progress in Materials Science 51 (2006) 881–981.
[32] H. Conrad, Grain size dependence of the plastic deformation kinetics in Cu, Materials Science and Engineering A 341 (2003) 216–228.
[33] M. Richert, Features of cyclic extrusion compression method, structure & materials properties, Solid State Phenomena 114 (2006) 19–28.
[34] Y. Huang, T.G. Langdon, Advances in ultrafine-grained materials, Materials Today 16 (2013) 85–93.
[35] R.S. Mishra, M.W. Mahoney, Friction Stir Welding and Processing, ASM International, Materials Park, 2007.
[36] M.St. Węglowski, P. Sedek, C. Hamilton, Experimental analysis of residual stress in friction stir processed cast AlSi9Mg aluminium alloy, Key Engineering Materials 682 (2016) 18–23.
[37] A. Yazdipour, A.M. Shafiei, K. Dehghani, Modeling the microstructural evolution and effect of cooling rate on the nanograins formed during the friction stir processing of Al5083, Materials Science and Engineering A 527 (2009) 192–197.
[38] Z.W. Chen, S. Cui, W. Gao, T. Zhu, Microstructure development during friction stir processing of Al-7Si-0.3Mg cast alloy, in: 8th International Friction Stir Welding Symposium, Timmendorfer Strand, Germany, 18–20 May 2010, (2010) 1–8.
[39] R.M. Leal, I. Galvão, A. Loureiro, D.M. Rodrigues, Effect of friction stir processing parameters on the microstructural and electrical properties of copper, The International Journal of Advanced Manufacturing Technology 80 (2015) 1655–1663.
[40] D.U. XH, W.U. BaoLin, Using two-pass friction stir processing to produce nanocrystalline microstructure in AZ61magnesium alloy, Science in China Series E: Technological Sciences 52 (2009) 1751–1755.
[41] F.C. Liu, M.J. Tan, et al., Microstructural evolution and superplastic behavior in friction stir processed Mg–Li–Al–Zn alloy, Journal of Materials Science 48 (2013) 8539–8546.
[42] A.G. Rao, K.R. Ravi, B. Ramakrishnara, et al., Recrystallization phenomena during friction stir processing of hypereutectic aluminum-silicon alloy, Metallurgical and Materials Transactions A 44 (2012) 1519–1529.
[43] K.N. Ramesh, S. Pradeep, V. Pancholi, Multipass friction-stir processing and its effect on mechanical properties of aluminum alloy 5086, Metallurgical and Materials Transactions A 43 (2012) 4311–4319.
[44] M.St. Węglowski, M. Kopyściański, S. Dymek, Friction stir processing multi-run modification of cast aluminum alloy, Key Engineering Materials 611-612 (2014) 1595–1600.
[45] Y.J. Kwon, M. Saito, I. Shigematsu, Friction stir process as a new manufacturing technique of ultrafine grained aluminum alloy, Journal of Materials Science Letters 21 (2002) 1473– 1476.
[46] H.S. Grewal, H.S. Arora, et al., Surface modification of hydroturbine steel using friction stir processing, Applied Surface Science 268 (2013) 547–555.
[47] C.I. Chang, X.H. Du, et al., Achieving ultrafine grain size in Mg–Al–Zn alloy by friction stir processing, Scripta Materialia 57 (2007) 209–212.
[48] N. Kumar, R.S. Mishra, Ultrafine-grained Al-Mg-Sc alloy via friction-stir processing, Metallurgical and Materials Transactions A 44 (2012) 934–945.
[49] M. Barmouz, M.K.B. Givi, J. Jafari, Evaluation of tensile deformation properties of friction stir processed pure copper: effect of processing parameters and pass number, Journal of Materials Engineering and Performance 23 (2014) 101–107.
[50] M. Kopyściański, M.St. Węglowski, et al., Electron microscopy investigation of a cast AlSi9Mg aluminum alloy subjected to friction stir processing with overlapping passes, International Journal of Materials Research 106 (2015) 813–817.
[51] H.S. Arora, H. Singh, B.K. Dhindaw, Some observations on microstructural changes in a Mg-based AE42 alloy subjected to friction stir processing, Metallurgical and Materials Transactions B 43 (2011) 92–108.
[52] J. Li, D.T. Zhang, F. Chai, W. Zhang, Microstructures and mechanical properties of WE43 magnesium alloy prepared by friction stir processing, Rare Metals (2014), http://dx.doi.org/10.1007/s12598-014-0306-3 (Forthcoming).
[53] N. Yasavol, H. Jafari, Microstructure, mechanical and corrosion properties of friction stir-processed AISI D2 tool steel, Journal of Materials Engineering and Performance 24 (2015) 2151–2157.
[54] M.J. Rubal, M.C. Juhas, J.C. Lippold, Microstructure evolution during friction stir processing of Ti-5111, in: 8th International Symposium on Friction Stir Welding, Timmendorfer Strand, Germany, 18–20 May 2010, (2010) 190–203.
[55] C.J. Lee, J.C. Huang, P.J. Hsieh, Mg based nano-composites fabricated by friction stir processing, Scripta Materialia 54 (2006) 1415–1420.
[56] Y. Morisada, H. Fujii, T. Nagaoka, M. Fukusumi, Nanocrystallized magnesium alloy – uniform dispersion of C60 molecules, Scripta Materialia 55 (2006) 1067–1070.
[57] Y. Morisada, H. Fujii, T. Nagaoka, M. Fukusumi, Effect of friction stir processing with SiC particles on microstructure and hardness of AZ31, Materials Science and Engineering A 433 (2006) 50–54.
[58] Y. Morisada, H. Fujii, T. Nagaoka, M. Fukusumi, MWCNTs/AZ31 surface composites fabricated by friction stir processing, Materials Science and Engineering A 419 (2006) 344–348.
[59] P. Asadi, G. Faraji, M.K. Besharati, Producing of AZ91/SiC composite by friction stir processing (FSP), The International Journal of Advanced Manufacturing Technology 51 (2010) 247–260.
[60] M. Azizieh, A.H. Kokabi, P. Abachi, Effect of rotational speed and probe profile on microstructure and hardness of AZ31/Al2O3 nanocomposites fabricated by friction stir processing, Materials and Design 32 (2011) 2034–2041.
[61] G. Faraji, O. Dastani, S.A.A.A. Mousavi, Effect of process parameters on microstructure and micro-hardness of AZ91/Al2O3 surface composite produced by FSP, Journal of Materials Engineering and Performance 20 (2011) 1583–1590.
[62] D. Khayyamin, A. Mostafapour, R. Keshmiri, The effect of process parameters on microstructural characteristics of

AZ91/SiO2 composite fabricated by FSP, Materials Science and Engineering A 559 (2013) 217–221.
[63] M. Golmohammadi, M. Atapour, A. Ashrafi, Fabrication and wear characterization of an A413/Ni surface metal matrix composite fabricated via friction stir processing, Materials and Design 85 (2015) 471–482.
[64] L.B. Johannes, L.L. Yowell, et al., Survivability of single-walled carbon nanotubes during friction stir processing, Nanotechnology 17 (2006) 3081–3084.
[65] S.M. Howard, B.K. Jasthi, et al., Friction surface reaction processing in aluminium substrates, in: Friction Stir Welding and Processing III TMS Annual Meeting, San Francisco, (2005) 139–146.
[66] R.S. Mishra, Z.Y. Ma, et al., Friction stir processing: a novel technique for fabrication of surface composite, Materials Science and Engineering A 341 (2003) 307–310.
[67] E.R.I. Mahmoud, M. Takahashi, T. Shibayanagi, K. Ikeuchi, Effect of friction stir processing tool probe on fabrication of SiC particle reinforced composite on aluminium surface, Science and Technology of Welding and Joining 14 (2009) 413–425.
[68] E.R.I. Mahmoud, K. Ikeuchi, M. Takahashi, Fabrication of SiC particle reinforced composite on aluminium surface by friction stir processing, Science and Technology of Welding and Joining 13 (2008) 607–618.
[69] S.A. Alidokht, A. Abdollah-zadeh, et al., Microstructure and tribological performance of an aluminium alloy based hybrid composite produced by friction stir processing, Materials and Design 32 (2011) 2727–2733.
[70] A. Dolatkhah, P. Golbabaei, et al., Investigating effects of process parameters on microstructural and mechanical properties of Al5052/SiC metal matrix composite fabricated via friction stir processing, Materials and Design 37 (2012) 458–464.
[71] E.R.I. Mahmoud, M. Takahashi, et al., Fabrication of surface-hybrid-MMCs layer on aluminum plate by friction stir processing and its wear characteristics, Materials Transactions 50 (2009) 1824–1831.
[72] C.M. Maxwell Rejil, et al., Microstructure and sliding wear behavior of AA6360/(TiC + B4C) hybrid surface composite layer synthesized by friction stir processing on aluminum substrate, Materials Science and Engineering A 552 (2012) 336–344.
[73] S. Soleymani, A. Abdollah-zadeh, S.A. Alidokht, Microstructural and tri-bological properties of Al5083 based surface hybrid composite produced by friction stir processing, Wear 278 (2012) 41–47.
[74] B. Zahmatkesh, M.H. Enayati, A novel approach for development of surface nanocomposite by friction stir processing, Materials Science and Engineering A 527 (2010) 6734–6740.
[75] A. Shafiei-Zarghani, S.F. Kashani-Bozorg, A. Zarei-Hanzaki, Microstructures and mechanical properties of Al/$Al_2O_3$ surface nano-composite layer produced by friction stir processing, Materials Science and Engineering A 500 (2009) 84–91.
[76] M. Zohoor, M.K.B. Givi, P. Salami, Effect of processing parameters on fabrication of Al-Mg/Cu composites via friction stir processing, Materials and Design 39 (2012) 358–365.
[77] M. Barmouz, M.K.B. Givi, J. Seyfi, On the role of processing parameters in producing Cu/SiC metal matrix composites via friction stir processing: Investigating microstructure, microhardness, wear and tensile behavior, Materials Characterization 62 (2011) 108–117.
[78] M. Barmouz, M.K.B. Givi, Fabrication of in situ Cu/SiC composites using multi-pass friction stir processing: evaluation of microstructural, porosity, mechanical and electrical behavior, Composites Part A: Applied Science and Manufacturing 42 (2011) 1445–1453.
[79] R. Sathiskumar, N. Murugan, I. Dinaharan, S.J. Vijay, Characterization of boron carbide particulate reinforced in situ copper surface composites synthesized using friction stir processing, Materials Characterization 84 (2013) 16–27.
[80] M. Barmouz, J. Seyfi, M.K.B. Givi, I. Hejazi, S. Davachi, A novel approach for producing polymer nanocomposites by in-situ dispersion of clay particles via friction stir processing, Materials Science and Engineering A 528 (2011) 3003–3006.
[81] A. Ghasemi-Kahrizsangi, S.F. Kashani-Bozorg, Microstructure and mechanical properties of steel/TiC nano-composite surface layer produced by friction stir processing, Surface and Coatings Technology 209 (2012) 15–22.
[82] A. Ghasemi-Kahrizsangi, S.F. Kashani-Bozorg, M. Moshref-Javadi, Effect of friction stir processing on the tribological performance of Steel/Al2O3 nanocomposites, Surface and Coatings Technology 276 (2015) 507–515.
[83] A. ShamsipurA, S.F. Kashani-Bozorg, A. Zarei-Hanzaki, The effects of friction-stir process parameters on the fabrication of Ti/SiC nano-composite surface layer, Surface and Coatings Technology 206 (2011) 1372–1381.
[84] A. Shamsipur, et al., Production of in-situ hard Ti/TiN composite surface layers on CP-Ti using reactive friction stir processing under nitrogen environment, Surface and Coatings Technology 218 (2013) 62–70.
[85] A. Shafiei-Zarghani, S.F. Kashani-Bozorg, A.P. Gerlich, Strengthening analyses and mechanical assessment of Ti/Al2O3 nano-composites produced by friction stir processing, Materials Science and Engineering A 631 (2015) 75–85.
[86] V. Sharma, U. Prakash, et al., Surface composites by friction stir processing: a review, Journal of Materials Processing Technology 224 (2002) 117–134.
[87] D.K. Lim, T. Shibayanagi, A.P. Gerlich, Synthesis of multi-walled CNT reinforced aluminium alloy composite via friction stir processing, Materials Science and Engineering A 507 (2009) 194–199.
[88] M.N. Avettand-Fènoël, A. Simar, R. Shabadi, R. Taillard, B. de Meester, Characterization of oxide dispersion strengthened copper based materials developed by friction stir processing, Material Design 60 (2014) 343–357.
[89] Y. Huang, Y. Wang, et al., Microstructure and surface mechanical property of AZ31 Mg/SiCp surface composite fabricated by direct friction stir processing, Materials and Design 59 (2014) 274–278.
[90] R.M. Miranda, T.G. Santos, et al., Reinforcement strategies for producing functionally graded materials by friction stir processing in aluminium alloys, Journal of Materials Processing Technology 213 (2013) 1609–1615.
[91] Y. Mazaheri, F. Karimzadeh, M.H. Enayati, A novel technique for development of A356/Al2O3 surface nanocomposite by friction stir processing, Journal of Materials Processing Technology 211 (2011) 1614–1619.
[92] R. Bauri, D. Yadav, G. Suhas, Effect of friction stir processing (FSP) on microstructure and properties of Al–TiC in situ composite, Materials Science and Engineering A 528 (2011) 4732–4739.
[93] H. Farnoush, A. Sadeghi, et al., An innovative fabrication of nano-HA coatings on Ti-CaP nanocomposite layer using a combination of friction stir processing and electrophoretic deposition, Ceramics International 39 (2013) 1477–1483.
[94] F. Khodabakhshi, A.P. Gerlich, A. Simchi, A.H. Kokabi, Cryogenic friction-stir processing of ultrafine-grained Al–Mg–$TiO_2$ nanocomposites, Materials Science and Engineering A 620 (2015) 471–482.
[95] B. Li, Y. Shen, L. Luo, W. Hu, Fabrication of TiCp/Ti–6Al–4V surface composite via friction stir processing (FSP): process optimization, particle dispersion-refinement behavior and

hardening mechanism, Materials Science and Engineering 574 (2013) 75–85.
[96] J. Qian, J. Li, et al., In situ synthesizing Al3Ni for fabrication of intermetallic-reinforced aluminum alloy composites by friction stir processing, Materials Science and Engineering A 550 (2012) 279–285.
[97] A. Kurt, I. Uygur, E. Cete, Surface modification of aluminium by friction stir processing, Journal of Materials Processing Technology 211 (2011) 313–317.
[98] R. Rai, A. De, H.K.D.H. Bhadeshia, T. DebRoy, Review: friction stir welding tools, Science and Technology of Welding and Joining 16 (2011) 325–342.
[99] C.M. Chen, R. Kovacevic, Joining of Al 6061 alloy to AISI 1018 steel by combined effects of fusion and solid state welding, International Journal of Machine Tools and Manufacture 44 (2004) 1205–1214.
[100] G.K. Padhy, C.S. Wu, S. Gao, Auxiliary energy assisted friction stir welding – status review, Science and Technology of Welding and Joining 20 (2015) 631–649.
[101] K. Park, Development and analysis of ultrasonic assisted friction stir welding process, (Doctoral Thesis), The University of Michigan, 2009.
[102] A. Rusinko, Analytical description of ultrasonic hardening and softening, Ultrasonics 51 (2011) 709–714.
[103] J. Hung, C. Lin, Investigations on the material property changes of ultrasonic vibration assisted aluminum alloy upsetting, Materials and Design 45 (2013) 412–420.
[104] S. Kumar, C.S. Wu, G.K. Padhy, W. Ding, Application of ultrasonic vibrations in welding and metal processing: a status review, Journal of Manufacturing Processes 26 (2017) 295–322.
[105] L. Ruilin, H. Diqiu, L. Luocheng, Y. Shaoyong, Y. Kunyu, A study of the temperature field during ultrasonic-assisted friction-stir welding, The International Journal of Advanced Manufacturing Technology 73 (2014) 321–327.
[106] H. Ma, D. He, J. Liu, Ultrasonically assisted friction stir welding of aluminium alloy 6061, Science and Technology of Welding and Joining 20 (2015) 216–221.
[107] B. Strass, G. Wagner, D. Eifler, Realization of Al/Mg-hybrid joints by ultrasound supported friction stir welding, Materials Science Forum 783–786 (2014) 1814–1819.
[108] X.C. Liu, C.S. Wu, G.K. Padhy, Improved weld macrosection, microstructure and mechanical properties of 2024Al-T4 butt joints in ultrasonic vibration enhanced friction stir welding, Science and Technology of Welding and Joining 20 (2015) 345–352.
[109] R.F. Zinati, Experimental evaluation of ultrasonic-assisted friction stir process effect on in situ dispersion of multi-walled carbon nanotubes throughout polyamide 6, The International Journal of Advanced Manufacturing Technology 81 (2015) 2087–2098.
[110] S. Kumar, Ultrasonic assisted friction stir processing of 6063 aluminum alloy, Archives of Civil and Mechanical Engineering 16 (2016) 473–484.